Band-gap boundaries and fundamental solitons in complex two-dimensional nonlinear lattices

Mark J. Ablowitz
Department of Applied Mathematics, University of Colorado, Colorado 80309-0526, USA

Nalan Antar and İlkay Bakırtaş
Istanbul Technical University, Maslak 34469, Istanbul, Turkey

Boaz Ilan
School of Natural Sciences, University of California at Merced, Merced, California 95344, USA

(Received 9 November 2009; published 22 March 2010)

Nonlinear Schrödinger (NLS) equation with external potentials (lattices) possessing crystal and quasicrystal structures are studied. The fundamental solitons and band gaps are computed using a spectral fixed-point numerical scheme. Nonlinear and linear stability properties of the fundamental solitons are investigated by direct simulations and the linear stability properties of the fundamental solitons are confirmed by analysis the linearized eigenvalue problem.

DOI: 10.1103/PhysRevA.81.033834 PACS number(s): 42.65.Tg

I. INTRODUCTION

Solitons are localized nonlinear waves and occur in many branches of physics. Their properties have provided fundamental understanding of complex nonlinear systems. In recent years there has been considerable interest in studying solitons in system with periodic potentials or lattices, in particular, those that can be generated in nonlinear optical materials [1–5]. In periodic lattices, solitons can typically form when their propagation constant (or eigenvalue) is within certain region, so-called gaps, a concept that is borrowed from the Floquet-Bloch theory for linear propagation. However, the external potential of complex systems can be much more general and physically richer than a periodic lattice. For example, atomic crystals can have various irregularities, such as defects and edge dislocations and also quasicrystal structures, which have long-range orientational order but no translational symmetry [6–8]. In general, when the lattice periodicity is slightly perturbed, the band-gap structure and soliton properties also become slightly perturbed, and solitons are expected to exist in much the same as in the perfectly periodic case [9,10]. On the other hand, little known about the spectrum with quasiperiodic potential (cf. Ref. [11]).

In this study, we investigate the fundamental solitons in lattices that have periodic and quasicrystal structures. The model is the following focusing nonlinear $(2+1)D$ nonlinear Schrödinger (NLS) equation with an external potential

$$iu_z + \Delta u + |u|^2 u - V(x,y)u = 0. \tag{1}$$

In optics, $u(x,y,z)$ corresponds to the complex-valued, slowly varying amplitude of the electric field in the xy plane propagating in the z direction, $\Delta u \equiv u_{xx} + u_{yy}$ corresponds to diffraction, the cubic term in u originates from the nonlinear (Kerr) change of the refractive index and $V(x,y)$ is an external optical potential that can be written as the intensity of a sum of N phase-modulated plane waves (see Ref. [12]), i.e.,

$$V(x,y) = \frac{V_0}{N^2}\left|\sum_{n=0}^{N-1} e^{i(k_x x + k_y y)}\right|^2, \tag{2}$$

where $V_0 > 0$ is constant and corresponds to the peak depth of the potential, i.e., $V_0 = \max_{x,y} V(x,y)$. In this study, we seek a soliton solution of Eq. (1) in the form $u(x,y,z) = f(x,y)e^{-i\mu z}$, where $f(x,y)$ is a real valued function and μ is the propagation constant (eigenvalue). Substituting this form of solution into Eq. (1), the following nonlinear eigenequation is obtained

$$\Delta f + [\mu + |f|^2 - V(x,y)]f = 0. \tag{3}$$

We use a fixed-point spectral computational method (spectral renormalization method) to solve Eq. (3) as explained below. After applying the Fourier transformation to Eq. (3), we add and subtract a term $r\hat{f}$, where $r > 0$. This procedure leads us to the following equation

$$\hat{f}(\nu) = \hat{R}[\hat{f}] \equiv \frac{(r+\mu)\hat{f} + \mathcal{F}\{[|f|^2 - V(x,y)]f\}}{r + |\nu|^2}. \tag{4}$$

Here $\mathcal{F}$ denotes the Fourier transformation, $\nu = (\nu_x, \nu_y)$ are Fourier variables and r is used to avoid singularity in the denominator. We introduce a new field variable $f(x,y) = \lambda w(x,y)$, where $\lambda \neq 0$ is a constant to be determined. The iteration method takes the form $\hat{w}_{m+1} = \lambda_m^{-1}\hat{R}[\lambda_m \hat{w}_m]$, $m = 0, 1, 2, \ldots$, where λ_m satisfies the associated algebraic condition

$$\iint_{-\infty}^{+\infty} |\hat{w}_m(\nu)|^2 d\nu = \lambda_m^{-1} \iint_{-\infty}^{+\infty} \hat{R}[\lambda_m \hat{w}_m]\hat{w}_m^*(\nu)d\nu. \tag{5}$$

It has been found that this method often prevents the numerical scheme from diverging. Thus, the soliton is obtained from a convergent iterative scheme. The initial starting point $w_0(x,y)$ is typically chosen to be a Gaussian centered around one of the lattice's critical points. The iteration continues until $|w_{m+1} - w_m| < 10^{-10}$ and the relative error $\delta = |\lambda_{m+1}/\lambda_m - 1|$ reaches 10^{-10}. Convergence is usually obtained quickly when the mode is strongly localized in the band gap called semi-infinite band gap. Further, it is observed that the mode becomes more extended as μ gets closer to the band gap edge and convergence of such a mode slows down during the iterations.

In this work, we computed the fundamental solitons on the periodic and quasicrystal lattices by using the spectral renormalization method explained above. We investigated the first band-gap structures for with external potentials [$N =$ 2–7 in Eq. (2)]. The nonlinear and linear stability of the fundamental solitons are studied by direct computations of Eq. (1) using quasicrystal and periodic potentials, where the initial conditions are taken to be the fundamental solitons with 1% random complex noise. Linear stability is also studied via the linear eigenvalue problem. The results are consistent with those obtained by direct simulation.

II. BAND-GAP STRUCTURES AND LINEAR SPECTRUM

If the nonlinear term $|u|^2 u$ is ignored in Eq. (1) and the potential is assumed to be periodic, i.e., $V(\vec{x}) = V(\vec{x} + \vec{L})$, then looking for solutions in the form $u(x,y,z) = f(x,y)e^{-i\mu z}$ leads us to the following eigenequation

$$\Delta f + [\mu - V(\vec{x})]f = 0. \tag{6}$$

According to the Floquet-Bloch theory, Eq. (6) has a solution given as

$$f(\vec{x}) = e^{i\vec{k}\cdot\vec{x}} p(\vec{x}), \tag{7}$$

where $p(\vec{x}) = p(\vec{x} + \vec{L})$ is a bounded function with the same periodicity as the potential $V(\vec{x})$.

If the potential is separable, i.e.,

$$V(X,Y) = V_0(\cos^2 X + \cos^2 Y), \tag{7a}$$

then the dimensionality of the problem is reduced and Eq. (1) can be split into two Mathieu's equations whose band-gap structure are well known. Musslimani and Yang [13] compared the band-gap structures of the linear periodic problem by using Floquet-Bloch theory and perturbation theory at small V_0 values. They found that for the first band gap, the band-gap boundaries obtained from Mathieu's equation and leading-order approximations from perturbation theory

$$\mu \approx V_0 - 1/16{V_0}^2 \tag{7b}$$

are in good agreement.

In Fig. 1, we demonstrate a comparison of the first band gap boundary of the linear periodic problem obtained by Musslimani and Yang [13] and the boundary obtained for the nonlinear problem by using spectral renormalization outlined in Sec. I. The first band gap is the edge of the parameter regime of the potential depth V_0 and eigenvalue μ in which the numerical method converges to a localized mode. In the band-gap region, while keeping the same potential depth V_0, beyond a certain threshold value of the eigenvalue μ, the numerical method yields to an extended state which is called the Bloch wave region.

As can be seen in the figure, the band-gap boundaries of both cases are close to each other.

III. PERIODIC AND QUASICRYSTAL POTENTIALS

In this section, we investigate 2D solitons on periodic and quasicrystal lattices. In certain materials, these type of lattices appear naturally and they can be generated artificially by the use of laser beams in optical experiments.

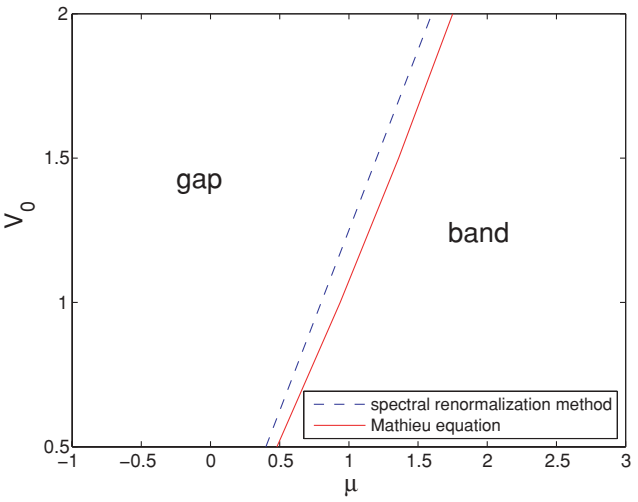

FIG. 1. (Color online) A comparison of the first band-gap boundary of Mathieu's equation obtained from Eq. (6) and the spectral renormalization method for the NLS Eq. (1).

In this study, the formulation of such a potential is given as follows:

$$V_N(x,y) = \frac{V_0}{N^2}\left|\sum_{n=0}^{N-1} e^{i(k_x x + k_y y)}\right|^2, \tag{8}$$

where $(k_x, k_y) = [K\cos(2\pi n/N), K\sin(2\pi n/N)]$, where we choose $K = 2\pi$.

The potentials for $N = 2, 3, 4, 6$ yield periodic lattices that correspond to standard 2D crystal structures, whereas $N =$ 5, 7 correspond to quasicrystals. In particular, the quasicrystal with $N = 5$ is often called the Penrose tiling. In Fig. 2, contour images of the lattices $N = 2$–7, all with $V_0 = 2$, $K = 2\pi$, are displayed. Recently, Freedman *et al.* observed solitons in Penrose and other quasicrystal lattices generated by the optical induction method [14].

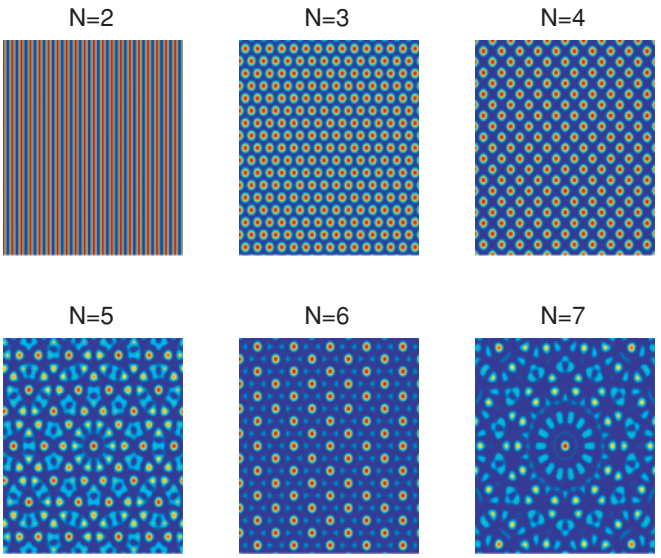

FIG. 2. (Color online) Contour images of the lattices, all with $V_0 = 2$, $K = 2\pi$.

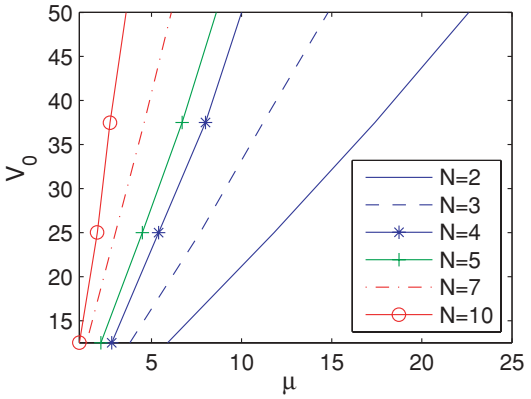

FIG. 3. (Color online) (a) Band-gap boundaries for NLS equation with the external potentials, $N = 2$–10.

The following initial condition in the spectral renormalization method

$$u(x,y) = e^{-[(x+x_0)^2+(y+y_0)^2]}$$

yields localized modes (solitons) on each lattice for $N = 2$–7. We remark that the origin is the global maximum of the lattice for all values of N.

To compare the first band-gap formation of each lattice, we set the potential depth V_0 to a fixed value (starting from 15 to 50). For each value of V_0, by increasing the μ values, we check both the convergence and the localization of the mode. When the mode becomes more extended, usually the convergence is slower and after a certain value of μ, typically both the convergence cannot be reached and the localization of the mode is lost. In this way we locate the boundary of the first band gap of the related lattice. The first band-gap boundaries for related crystals and quasicrystals are depicted in Fig. 3.

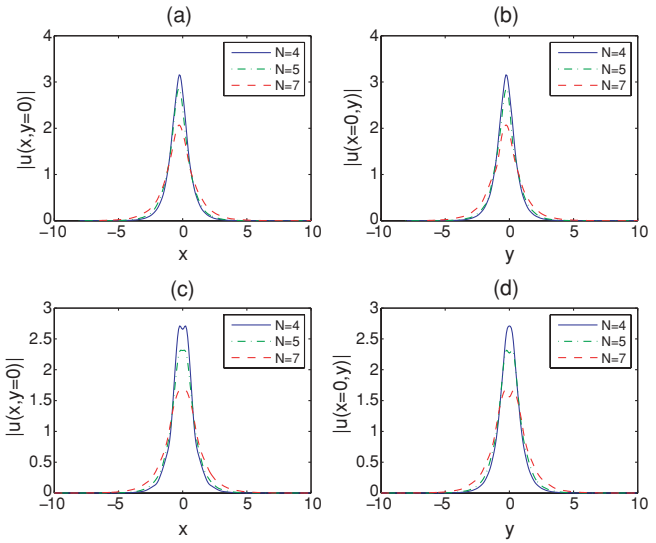

FIG. 4. (Color online) (Top) On-axis mode profiles for $N = 4, 5, 7$ (a) and (b) soliton centered at a potential minimum profile along the x and y axes. [(c) and (d)] Soliton centered at a potential maximum profile along the x and y axes.

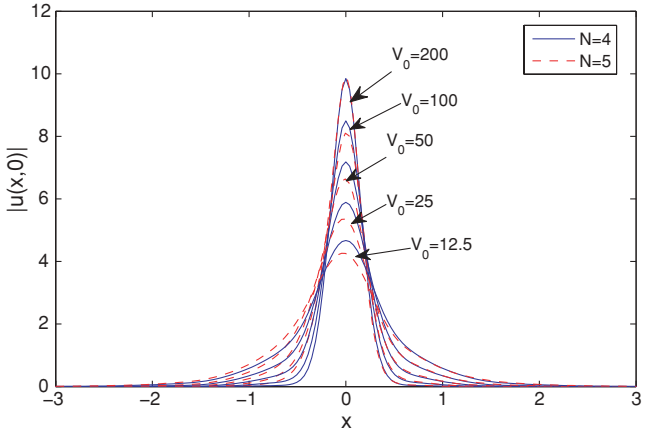

FIG. 5. (Color online) The mode profile for periodic ($N = 4$) and Penrose ($N = 5$) potentials.

As can be seen from the figure, as the number of points N decreases, the first band gap of the corresponding lattice enlarges. Another interesting phenomena occurs in the investigation of the slopes of those band-gap boundaries. It can be seen that, as number of points increases, the slope of the related band gap boundary of the lattice increases. In the limit $N \to \infty$, the corresponding lattice is called Bessel lattice $V_\infty = (J_0(kr))^2$. Kartashov, Vysloukh, and Torner investigate the basic properties and linear stability of optical solitons on radial-symmetric Bessel lattice in cubic nonlinear media [15].

As seen from Fig. 3(a) as N increases, the gap edge decreases and

$$\mu_{\max}[V_N] \to +0, \quad N \to \infty. \tag{9}$$

To compare the mode profiles of crystals and quasicrystals, we plotted the on axis mode profile for $N = 4, 5$ and $N = 7$. As suggested in Fig. 4 as N increases the amplitudes of the fundamental solitons decrease.

When we increased the depth of potential from 12.5 to 100, interestingly the fundamental mode of the Penrose lattice approaches the fundamental mode of the periodic lattice (see Fig. 5).

For the Penrose potential we found fundamental solitons centered near the origin, which is the global maximum of the lattice potential (see Fig. 6). The fundamental solitons on the lattice maxima have a dimple, whereas the fundamental

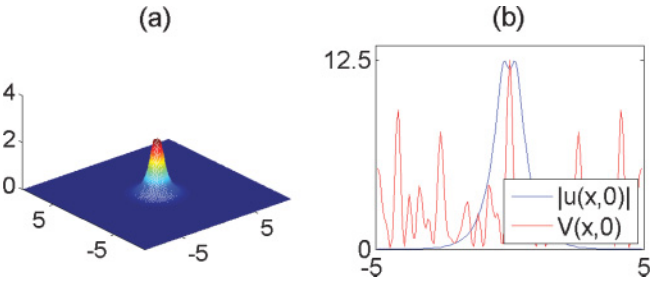

FIG. 6. (Color online) Soliton centered at the global maximum of Penrose lattice; (a) soliton intensity in a 3D view showing the dimple; (b) cross section along y axis of a Penrose soliton (solid line) superimposed on the underlying lattice (dashed line).

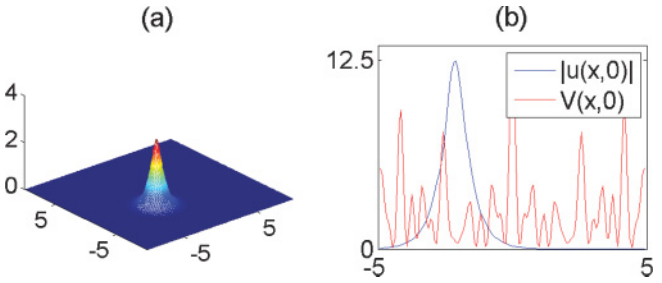

FIG. 7. (Color online) Soliton centered at the local minimum of Penrose lattice; (a) soliton intensity in 3D (no dimple); (b) cross section along y axis of a Penrose soliton (solid line) superimposed on the underlying lattice (dashed line).

solitons on the lattice minima do not have this dimple (see Fig. 7).

IV. NONLINEAR AND LINEAR STABILITY

A. Nonlinear stability

Now we address the critical question of nonlinear stability of the fundamental solitons. The power play an important role in determining the stability properties of the fundamental solitons. We define the power as

$$P = \int_{-\infty}^{\infty}\int_{-\infty}^{\infty} |u(x,y)|^2 dxdy. \tag{10}$$

An important analytic result on soliton stability was originally obtained by Vakhitov and Kolokolov [16]. They proved, by use of the linearized perturbation equation, that a necessary condition for linear stability was $dP/d\mu < 0$.

Key analytic results on soliton stability were obtained in Refs. [17,18]. They proved that the necessary conditions for orbital (nonlinear) stability are the slope condition, $dP/d\mu < 0$, and spectral condition, L_+ does not have more than one negative eigenvalue.

A necessary condition for collapse in the 2D cubic NLS equation is that the power of the beam exceeds the critical power $P_c \approx 11.7$ [19]. The fundamental solitons of NLS equation can become unstable in two ways: focusing instability or drift instability [20].

(a) If the slope condition is not satisfied, this leads to a focusing instability.

(b) The spectral condition is associated with the eigenvalue problem (see Ref. [20]). If the spectral condition is violated it

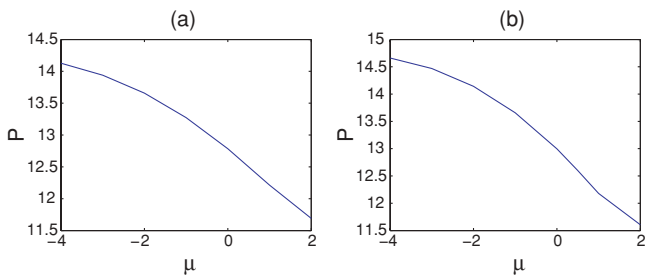

FIG. 8. (Color online) The power versus μ for (a) periodic potential ($N = 4$) with $V_0 = 12.5$; (b) Penrose potential ($N = 5$) with $V_0 = 12.5$ for solitons located on the lattice maxima.

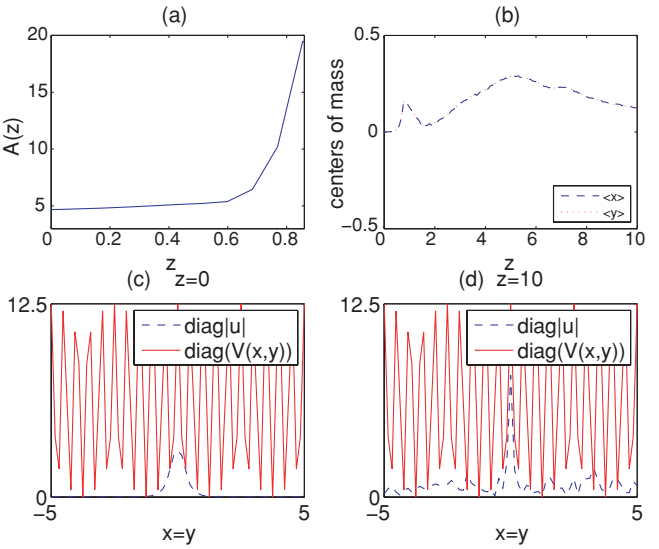

FIG. 9. (Color online) Evolution of soliton situated at the periodic potential with $V_0 = 12.5$ and $\mu = -3$. (a) Peak amplitude $A(z) = \max_{x,y}|\tilde{u}(x,y,z)|$ of the solution of Eq. (1) as a function of the propagation distance. The initial condition is taken as the fundamental soliton with a 0.01 noise in the amplitude and phase; (b) center-of-mass evolution in x and y coordinates; (c) cross section along the diagonal axis of a fundamental soliton at the maximum superimposed on the periodic potential at $z = 0$; (d) cross section along the diagonal axis of the fundamental soliton superimposed on the periodic potential after the propagation ($z = 10$).

leads to a drift instability, i.e., the fundamental soliton moves from the potential maximum toward a nearby lattice minimum.

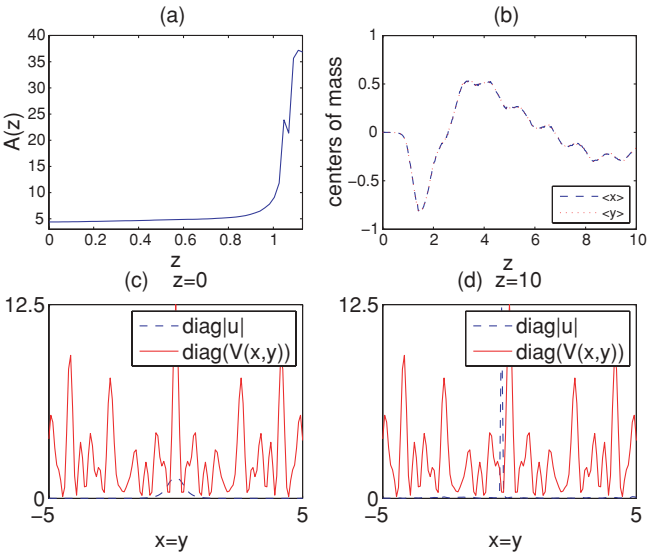

FIG. 10. (Color online) Evolution of soliton situated at the Penrose potential with $V_0 = 12.5$ and $\mu = -3$. (a) Peak amplitude $A(z) = \max_{x,y}|\tilde{u}(x,y,z)|$ of the solution of Eq. (1) as a function of the propagation distance. The initial condition is taken as the fundamental soliton with a 0.01 noise in the amplitude and phase; (b) center-of-mass evolution in x and y coordinates; (c) cross section along the diagonal axis of a fundamental soliton at the maximum superimposed on the periodic potential at $z = 0$; (d) cross section along the diagonal axis of the fundamental soliton superimposed on the periodic potential after the propagation ($z = 10$).

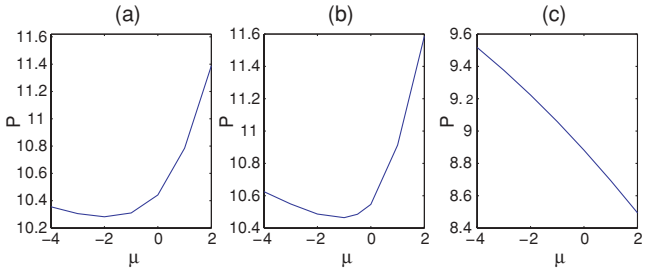

FIG. 11. (Color online) The power versus μ for (a) periodic potential with $V_0 = 12.5$; (b) Penrose potential with $V_0 = 12.5$; (c) Penrose potential with $V_0 = 50$.

Let us define the center of mass of a perturbed soliton as

$$\mathscr{C} = \frac{1}{P}\int_{-\infty}^{\infty}\int_{-\infty}^{\infty}(x+iy)|u|^2 dxdy \tag{11}$$

where the center of mass in x and y coordinates are defined as

$$\langle x\rangle := \text{real}(\mathscr{C}),\ \langle y\rangle := \text{imag}(\mathscr{C}). \tag{12}$$

To study the nonlinear stability, we directly compute Eq. (1) over a long distance (finite difference method was used on derivatives u_{xx} and u_{yy} and fourth-order Runge-Kutta method to advance in z) for both periodic and Penrose potentials. The inital conditions were taken to be a fundamental soliton with 1% random noise in the amplitude and phase. In this work, the nonlinear stability of the fundamental solitons located on the lattice maxima and minima are investigated in separate cases.

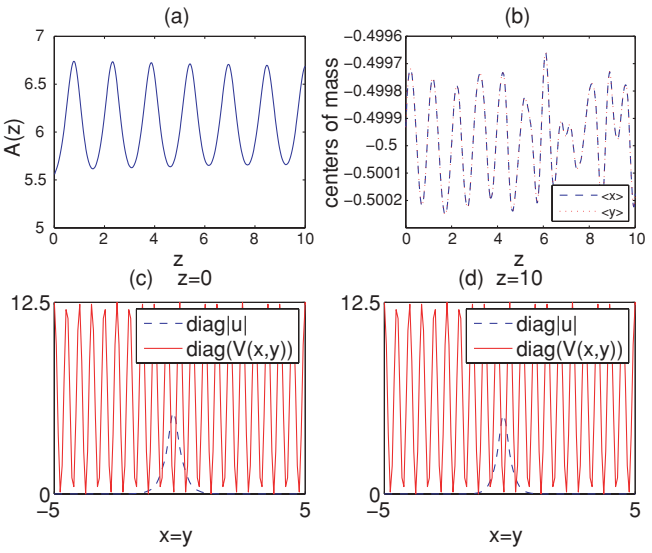

FIG. 12. (Color online) Evolution of soliton situated at the periodic potential with $V_0 = 12.5$ and $\mu = -3$. (a) Peak amplitude $A(z) = \max_{xy}|\tilde{u}(x,y,z)|$ of the solution of Eq. (1) as a function of the propagation distance. The initial condition is taken as the fundamental soliton with a 0.01 noise in the amplitude and phase; (b) center-of-mass evolution in x and y coordinates; (c) cross section along the diagonal axis of a fundamental soliton at the minimum superimposed on the periodic potential at $z = 0$; (d) cross section along the diagonal axis of the fundamental soliton superimposed on the periodic potential after the propagation ($z = 10$).

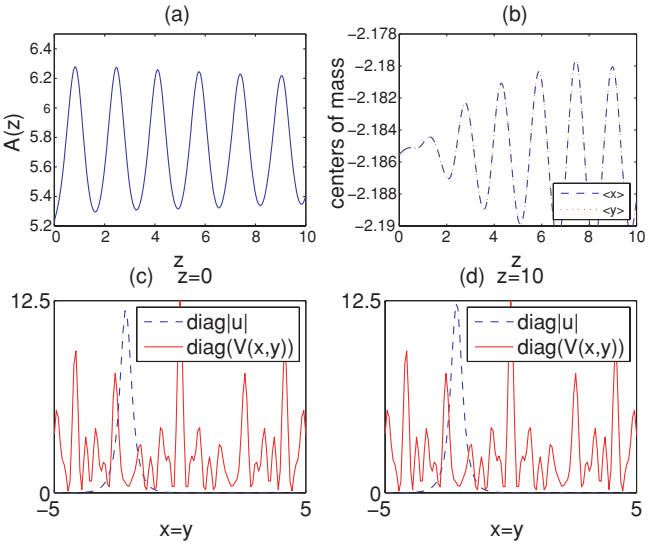

FIG. 13. (Color online) Evolution of soliton situated at the Penrose potential with $V_0 = 12.5$ and $\mu = -3$. (a) Peak amplitude $A(z) = \max_{xy}|\tilde{u}(x,y,z)|$ of the solution of Eq. (1) as a function of the propagation distance. The initial condition is taken as the fundamental soliton with a 0.01 noise in the amplitude and phase; (b) center-of-mass evolution in x and y coordinates; (c) cross section along the diagonal axis of a fundamental soliton at the minimum superimposed on the periodic potential at $z = 0$; (d) cross section along the diagonal axis of the fundamental soliton superimposed on Penrose potential after the propagation ($z = 10$).

B. Solitons on the lattice maxima

Once the solitons centered at the maxima are computed for a range of values of μ ($-4 \leqslant \mu \leqslant 2$), power versus μ graphs are plotted for both periodic and Penrose potentials. As seen from Fig. 8, the slope condition is satisfied for both periodic and Penrose potentials but the power exceeds the critical collapse value ($P_c = 11.72$) and collapse appears to be eventually attained.

In both Figs. 9 and 10, evolution of the fundamental solitons at the lattice maxima are plotted for the potential depth $V_0 = 12.5$ and $\mu = -3$. As can be seen from Fig. 9, the peak amplitude of the fundamental soliton $A(z) = \max_{xy}|\tilde{u}(x,y,z)|$ increases with the propagation distance z but the center of mass in the x and y axis Eq. (11) nearly stays at the same place. The fundamental soliton with periodic background is unstable nearly with focusing instability.

In Fig. 10, evolution of the fundamental soliton on the Penrose lattice maximum is plotted. The peak amplitude of the fundamental soliton stays the same for a while, then increases with propagation distance z. As opposed to Fig. 9, the center of mass moves from the global maximum of the lattice toward a nearby lattice minimum during the evolution. The fundamental soliton exhibits a drift instability.

C. Solitons on the lattice minima

We now investigate solitons centered at the lattice minima $(x_0, y_0) = (0.5, 0)$ for periodic potential and $(x_0, y_0) = (2.0918, 2.0918)$ for Penrose potential ($N = 5$). In Fig. 11, the power versus μ are depicted for periodic and Penrose

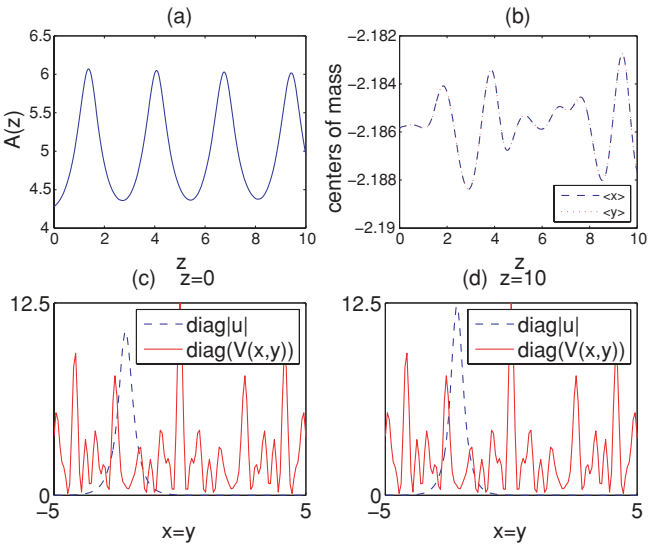

FIG. 14. (Color online) Evolution of soliton situated at the Penrose potential with $V_0 = 12.5$ and $\mu = -1$. (a) Peak amplitude $A(z) = \max_{xy}|\tilde{u}(x,y,z)|$ of the solution of Eq. (1) as a function of the propagation distance. The initial condition is taken as the fundamental soliton with a 0.01 noise in the amplitude and phase; (b) center-of-mass evolution in x and y coordinates; (c) cross section along the diagonal axis of a fundamental soliton at the minimum superimposed on the periodic potential at $z = 0$; (d) cross section along the diagonal axis of the fundamental soliton superimposed on Penrose potential after the propagation ($z = 10$).

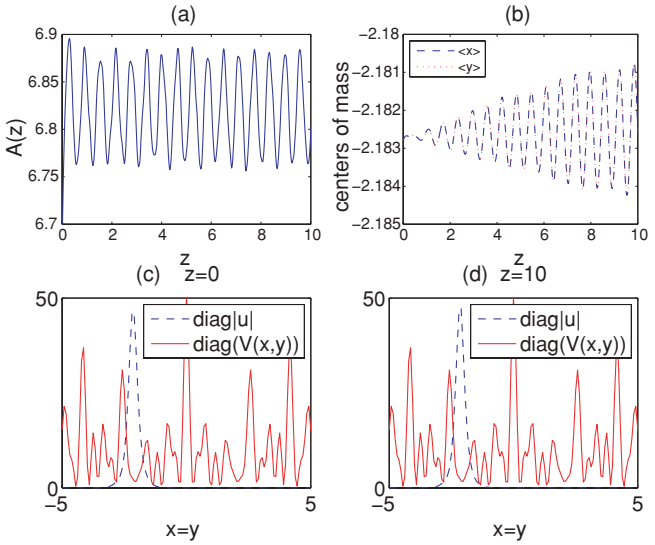

FIG. 15. (Color online) Evolution of soliton situated at the Penrose potential with $V_0 = 50$ and $\mu = -1$; (a) peak amplitude $A(z) = \max_{xy}|\tilde{u}(x,y,z)|$ of the solution of Eq. (1) as a function of the propagation distance. The initial condition is taken as the fundamental soliton with a 0.01 noise in the amplitude and phase; (b) center-of-mass evolution in x and y coordinates; (c) cross section along the diagonal axis of a fundamental soliton at the minimum superimposed on the periodic potential at $z = 0$; (d) cross section along the diagonal axis of the fundamental soliton superimposed on Penrose potential after the propagation ($z = 10$).

potential for various potential depths. Figure 11 shows that for the potential depth $V_0 = 12.5$, the slope condition is satisfied for both periodic and Penrose potentials below $\mu = -2$ but $\mu = -1$ is a saddle point and above $\mu = -1$ the slope condition is violated. When the potential depth is increased up to $V_0 = 50$ the slope condition is satisfied.

In both Figs. 12 and 13, evolution of the fundamental solitons at the lattice minima are plotted for the potential depth $V_0 = 12.5$ and $\mu = -3$. As can be seen from Figs. 12 and 13, peak amplitudes of the fundamental solitons $A(z) = \max_{xy}|\tilde{u}(x,y,z)|$ oscillate with the propagation distance z and the center of mass in the x and y axis nearly stay at the same place. This suggests that the fundamental solitons for both lattices are nonlinearly stable in this parameter regime.

Being a saddle point, the slope condition is violated at $\mu = -1$, $V_0 = 12.5$ for the Penrose potential. For small propagation distance the amplitude increases sharply (unstable) but then the peak amplitude oscillates and the center of mass stays nearly at the same place (see Fig. 14).

Figure 11 also shows that if the potential depth is increased up to $V_0 = 50$ the power versus μ graph has no saddle points and the slope condition is satisfied for $-4 \leqslant \mu \leqslant 2$. The fundamental soliton appears to be nonlinearly stable (see Fig. 15) in this parameter regime.

D. Linear stability

Now we address the critical question of linear stability of these fundamental solitons under kerr nonlinearity. For this, we linearized the Eq. (1) around the fundamental soliton. By denoting $u = \exp(-i\mu z)[u_0(x,y) + \tilde{u}(x,y,z)]$, where $u_0(x,y)$ is the fundamental soliton and $\tilde{u} \ll 1$ is the infinitesimal perturbation, the linearized equation for $\tilde{u}$ is

$$i\frac{\partial \tilde{u}}{\partial z} + \frac{\partial^2 \tilde{u}}{\partial x^2} + \frac{\partial^2 \tilde{u}}{\partial y^2} + (\mu - V(x,y) + 2|u_0|^2)\tilde{u} + u_0^2\tilde{u}^* = 0. \tag{13}$$

Starting from a white-noise initial condition, we simulated this linearized equation over a long distance (using finite differences on $\tilde{u}_{xx}$ and $\tilde{u}_{yy}$ and the fourth-order Runge-Kutta method to advance in z) for periodic and Penrose potentials.

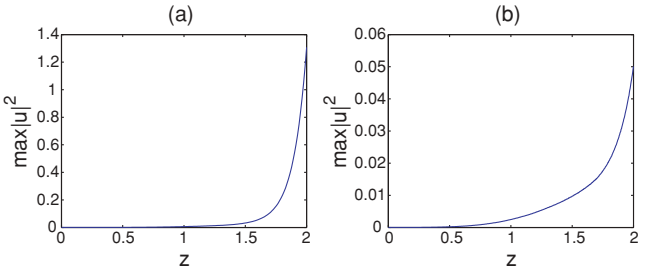

FIG. 16. (Color online) Dynamics of solutions of Eq. (13) with the periodic and Penrose potentials ($N = 5$). (a) Peak amplitude $A(z) = \max_{xy}|\tilde{u}(x,y,z)|$ of the solution as the function of z for periodic potential with $V_0 = 12.5$ and $\mu = -1$; (b) $A(z) = \max_{xy}|\tilde{u}(x,y,z)|$ of the solution as the function of z for Penrose potential with $V_0 = 12.5$ and $\mu = -1$; (c) $A(z) = \max_{xy}|\tilde{u}(x,y,z)|$ of the solution as the function of z for Penrose potential with $V_0 = 50$ and $\mu = -1$.

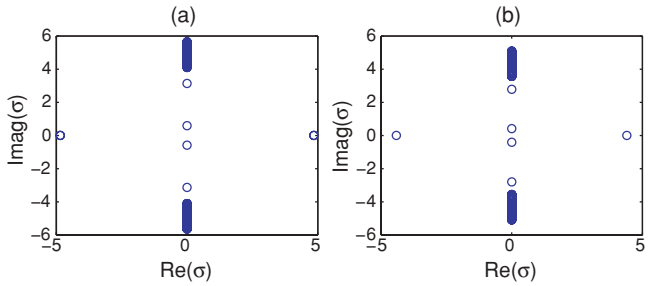

FIG. 17. (Color online) (a) Eigenvalues in the stability spectrum of the fundamental soliton centered at the lattice maximum for periodic potential with $V_0 = 12.5$ and $\mu = -1$; (b) eigenvalues in the stability spectrum of the fundamental soliton centered at the lattice maximum for Penrose potential ($N = 5$) with $V_0 = 12.5$ and $\mu = -1$.

If the solution grows exponentially then the fundamental soliton is considered to be linearly unstable. Otherwise, it is linearly stable. Following the procedure explained above, we observe only for some parameters linear stability of the fundamental mode (obtained by using the fixed-point iteration method).

In order to compare our results that obtained from the direct numerical simulations we also investigate the stability spectrum of the fundamental soliton. To study the spectrum of these fundamental solitons we assume that

$$\tilde{u}(x,y,z) = (v(x,y) + i\,w(x,y))e^{\sigma z} \tag{14}$$

Substituting this solution into Eq. (13) we obtain the following eigenvalue problem as

$$\begin{pmatrix} 0 & L_- \\ -L_+ & 0 \end{pmatrix} \begin{pmatrix} v \\ w \end{pmatrix} = \sigma \begin{pmatrix} v \\ w \end{pmatrix},$$

where L_- and L_+ are defined as

$$L_- = -\Delta - \left(\mu - V + u_0^2\right), \quad L_+ = -\Delta - \left(\mu - V + 3u_0^2\right).$$

Eigenvalues with positive real parts are unstable eigenvalues. The other eigenvalues are stable (purely imaginary

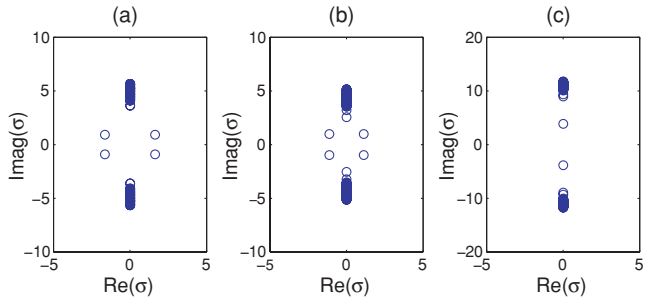

FIG. 18. (Color online) (a) Eigenvalues in the stability spectrum of the fundamental soliton centered at the lattice minimum for periodic potential with $V_0 = 12.5$ and $\mu = -1$; (b) eigenvalues in the stability spectrum of the fundamental soliton centered at the lattice minimum for Penrose potential ($N = 5$) with $V_0 = 12.5$ and $\mu = -1$; (c) eigenvalues in the stability spectrum of the fundamental soliton centered at the lattice minimum for Penrose potential ($N = 5$) with $V_0 = 50$ and $\mu = -1$.

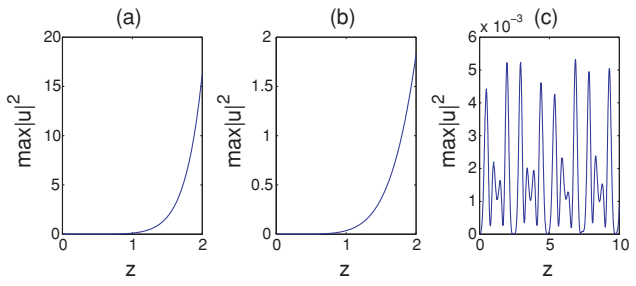

FIG. 19. (Color online) Dynamics of solutions of Eq. (13) with the periodic and Penrose potentials ($N = 5$). (a) Peak amplitude $A(z) = \max_{x,y}|\tilde{u}(x,y,z)|$ of the solution as the function of z for periodic potential with $V_0 = 12.5$ and $\mu = -1$; (b) peak amplitude $A(z) = \max_{x,y}|\tilde{u}(x,y,z)|$ of the solution as the function of z for Penrose potential with $V_0 = 12.5$ and $\mu = -1$; (c) peak amplitude $A(z) = \max_{x,y}|\tilde{u}(x,y,z)|$ of the solution as the function of z for Penrose potential with $V_0 = 50$ and $\mu = -1$.

eigenvalues are often called internal modes). We first investigate the linear stability of the fundamental soliton centered at the lattice maximum $(x_0, y_0) = (0, 0)$. We perform direct numerical simulations of Eq. (13) where the initial condition is 1% random noise within amplitude and phase. Figure 16 shows the maximum amplitude of the fundamental solitons for both periodic and Penrose potential versus the propagation distance z. As seen from these figures the maximum amplitudes of the fundamental solitons increase rapidly with increasing propagation constant. We also checked the linear eigenvalue problem for these fundamental solitons. We found that there are unstable ($\mathrm{Re}\sigma > 0$) eigenvalues (see Fig. 17). Thus, these fundamental solitons centered at the lattice maximum are linearly unstable.

We also investigate the linear stability of the fundamental soliton centered at lattice minima. In Fig. 16(a) the maximum amplitude of the fundamental soliton for periodic potential increase with the propagation distance z and there are eigenvalues with positive real part [see Fig. 18(a)]. Thus is seen to the fundamental soliton centered at the lattice mimina for periodic potential is linearly unstable. Also the fundamental mode associated with the Penrose potential for $V_0 = 12.5$ is not linearly stable. When we increased the depth of the potential as $V_0 = 50$ the fundamental mode with the Penrose potential is seen to be linearly stable. We verified these results with numerical simulations of the NLS equation and eigenvalue problem (see Figs. 18 and 19).

V. CONCLUSION

We have numerically demonstrated the existence of the fundamental solitons associated with both periodic and Penrose potentials. Using different types of quasicrystal structures ($N = 2$–7), the first band-gap formation for the NLS equation was determined. We investigated the nonlinear and linear stability properties of the fundamental solitons inside the first band gap for the periodic and Penrose potentials. Direct nonlinear numerical simulations of NLS equation show that when we put the initial conditions at the local maxima of the

lattices the fundamental solitons tends to collapse but solitons centered at the local minima oscillate with small amplitudes. Also we investigated the linear stability of the fundamental solitons and compared the results with eigenvalue problem. We verified the results with direct simulations for the linearized equation and the eigenvalue problem.

ACKNOWLEDGMENTS

This research was partially supported by the US Air Force Office of Scientific Research under Grant No. FA9550-09-1-0250. N. Antar was supported by Istanbul Technical University and İ. Bakırtaş was supported by TUBITAK.

[1] D. N. Christodoulides, F. Lederer, and Y. Silberberg, Nature **424**, 817 (2003).
[2] A. A. Sukhorukov, Y. S. Kivshar, H. S. Eisenberg, and Y. Silberberg, IEEE J. Quantum Electron. **39**, 31 (2003).
[3] N. K. Efremidis, J. Hudock, D. N. Christodoulides, J. W. Fleischer, O. Cohen, and M. Segev, Phys. Rev. Lett. **91**, 213906 (2003).
[4] J. W. Fleischer, M. Segev, N. K. Efremidis, and D. N. Christodoulides, Nature **422**, 147 (2003).
[5] D. Neshev, Y. S. Kivshar, H. Martin, and Z. Chen, Opt. Lett. **29**, 486 (2004).
[6] D. Shechtman, I. Blech, D. Gratias, and J. W. Cahn, Phys. Rev. Lett. **53**, 1951 (1984).
[7] M. Senechal, *Quasicrystals and Geometry* (Cambridge University Press, Cambridge, 1985).
[8] M. P. Marder, *Condensed Matter Physics* (Wiley, New York, 2000).
[9] F. Fedele, J. Yang, and Z. Chen, Stud. Appl. Math. **115**, 279 (2005).
[10] H. Buljan *et al.*, Stud. Appl. Math. **115**, 173 (2005).
[11] F. Roberta, J. Russell, and P. Raffaella, Nonlinear Anal. R. World Appl. **3**, 37 (2002).
[12] M. J. Ablowitz, B. Ilan, E. Schonbrun, and R. Piestun, Phys. Rev. E **74**, 035601(R) (2006).
[13] Z. H. Musslimani and J. Yang, J. Opt. Soc. Am. B **21**, 973 (2004).
[14] B. Freedman *et al.*, Nature **440**, 1166 (2006).
[15] Y. V. Kartashov, V. A. Vysloukh, and L. Torner, Phys. Rev. Lett. **93**, 093904 (2004).
[16] M. Vakhitov and A. Kolokolov, Radiophys. Quantum El. **16**, 783 (1973).
[17] M. I. Weinstein, SIAM J. Math. Anal. **16**, 472 (1985).
[18] H. A. Rose and M. I. Weinstein, Physica D **30**, 207 (1988).
[19] M. I. Weinstein, Commun. Math. Phys. **87**, 567 (1982).
[20] Y. Sivan, G. Fibich, B. Ilan, and M. I. Weinstein, Phys. Rev. E **78**, 046602 (2008).